COMPRESSED SENSING JOINT RANGE AND CROSS-RANGE MIMO RADAR IMAGING

Rafael Pinto and *Ricardo Merched*

Dept. of Electronics and Computer Engineering
Universidade Federal do Rio de Janeiro
rafaelgcpp@gmail.com, r.merched@gmail.com

ABSTRACT

Compressed sensing has proved key in resolving commonly sparse scenarios where MIMO Radar schemes are envisioned. This is normally addressed via cross-range imaging, equipped with a matched filter for each desired range. This paper takes a more general approach by formulating a full 3D convolution sensing matrix for joint range/cross-range imaging, while setting conditions for minimizing its corresponding mutual coherence. These conditions suggest that both the so-called complementary sequence sets, and manifold vectors allow for an extra degree of freedom in the design process. Simulations suggest that in comparison to independent Gaussian sequences, these complementary sets greatly improve robustness by reducing the system mutual coherence by an order of magnitude.

Index Terms— MIMO Radar, Compressed Sensing

1. INTRODUCTION

Multi-Input-Multi-Output (MIMO) radars have successfully improved parameter identifiability, resolution, and robustness, when compared to its single-antenna and phased-array counterparts [1],[2]. In such scenario, the received signal usually undergoes a bank of matched filters, whose delays are set in correspondence to the desired range bins, ultimately identifying the direction and reflectance of a given target. In this sense, range and cross-range parameters are commonly treated in separate, as in the developed models of [3] and [4], for example. While [3] designs complementary sequences sets for improving imaging performance via matched filtering and least-squares (LS) or Capon beamformation, [4] derives recovery conditions when imaging is addressed via compressed sensing (CS) matrices constructed by randomly located arrays (also via matched filtering).

In this context, the goal of this paper is to jointly construct the full range/cross-range convolution model for MIMO radars and obtain conditions for which the mutual coherence of the resulting sensing matrix is minimized. This is interpreted as a minimization of an upper-bound on the Rayleigh-Ritz quotients corresponding to several MIMO correlation lags, in which the involved array manifold vectors can be simultaneously designed to achieve this purpose. We remark that although [5] has followed a related approach towards a 3D MIMO radar design, it makes use of long Gaussian sequences which may demand a high level of synchronization, and only achieve good cross-correlation properties stochastically.The proposed model aims the imaging of static targets, commonly encountered in medical and geophysical scenes, and it does not take into account the Doppler effect. Simulations are included in order to verify the robustness of a CS formulation at different noise levels, and show that Gaussian sequences increase the mutual coherence by an order of magnitude.

2. MIMO RADAR SINGLE RANGE MODEL

Consider the MIMO radar model depicted in Fig. 1, consisting of an array of M_T isotropic transmitters, each positioned at $\mathbf{q}_m$, and a second array of M_R receivers, at positions denoted by $\tilde{\mathbf{q}}_n$. The antennas send narrowband pulses $p_i(t)$, with center frequency ω_0, through a homogeneous medium, which are scattered by K far-field targets with reflectance $\bar{s}_k$. These are located at a distance D, with directions given by unitary vectors denoted by $\bar{\mathbf{r}}_k$, which in turn are detected by the receiving array.

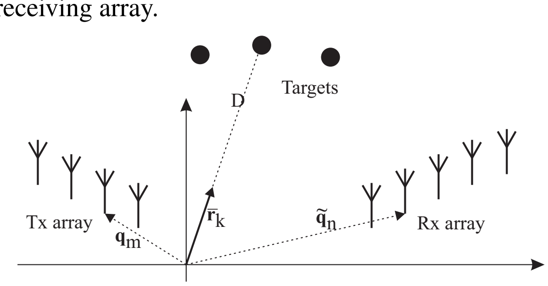

Fig. 1. Simplified schematic for a MIMO radar. All targets are located at the same range.

The manifold vectors [6] for the transmitting array are defined as

$$\mathbf{a}(\bar{\mathbf{r}}_k) = \begin{bmatrix} e^{j\frac{\omega_0}{c_0}\bar{\mathbf{r}}_k^T\mathbf{q}_0} & e^{j\frac{\omega_0}{c_0}\bar{\mathbf{r}}_k^T\mathbf{q}_1} & \dots & e^{j\frac{\omega_0}{c_0}\bar{\mathbf{r}}_k^T\mathbf{q}_{M_T-1}} \end{bmatrix}^T, \tag{1}$$

with analogous definition for the receiving manifold vector denoted by $\mathbf{b}(\bar{\mathbf{r}}_k)$, where $c_0 \triangleq \lambda_0/2\pi\omega_0$ is the speed of propagation for the medium.

Under the well known *Born* approximation [7], the received waveform can be written as:

$$\mathbf{y}_r(t) = \sum_{k=0}^{K-1} \bar{x}_k \mathbf{b}(\bar{\mathbf{r}}_k) \left[\mathbf{p}^T(t-2\tau_r)\mathbf{a}(\bar{\mathbf{r}}_k)\right] \ + \ \mathbf{n}(t) \quad (2)$$

where $\tau_r \triangleq D/c_0$, $\mathbf{n}(t)$ is an uncorrelated additive noise, and $\bar{x}_k$ is the free space path loss which we express as a corrected reflectance for the *k*-th target as

$$\bar{x}_k \triangleq -\frac{\omega_0^2}{16\pi^2 c_0^2 \tau_r^2}\bar{s}_k = -\frac{1}{4\lambda_0^2\tau_r^2}\bar{s}_k \, . \quad (3)$$

Also, the transmited pulse vector $\mathbf{p}(t)$ in (2) is denoted by

$$\mathbf{p}(t) \triangleq \begin{bmatrix} p_0(t) & p_1(t) & \cdots & p_{M_T-1}(t)\end{bmatrix}^T . \quad (4)$$

Sampling the received vector at t_s, i.e. $\mathbf{y}_r(n) \triangleq \mathbf{y}_r(2\tau_r+nt_s)$ and defining $\mathbf{p}(n) \triangleq \mathbf{p}(nt_s)$, we can rewrite (2) as

$$\begin{aligned}\mathbf{y}_r &\triangleq \begin{bmatrix}\mathbf{y}_r^T(N-1) & \mathbf{y}_r^T(N-2) & \cdots & \mathbf{y}_r^T(0)\end{bmatrix}^T & (5)\\ &= \sum_{k=0}^{K-1} \left[\mathbf{P}\mathbf{a}(\bar{\mathbf{r}}_k)\right] \otimes \mathbf{b}(\bar{\mathbf{r}}_k)\bar{x}_k \ + \ \mathbf{n} \, , & (6)\end{aligned}$$

where $\otimes$ represents the Kronecker product, and

$$\mathbf{P} = \begin{bmatrix} p_0(N-1) & p_1(N-1) & \cdots & p_{M_T-1}(N-1) \\ p_0(N-2) & p_1(N-2) & \cdots & p_{M_T-1}(N-2) \\ \vdots & \vdots & \vdots & \vdots \\ p_0(0) & p_1(0) & \cdots & p_{M_T-1}(0)\end{bmatrix} \quad (7)$$

is a $N \times M_T$ matrix representing the "unrolled" pulses which are N-samples long, and $\mathbf{n}$ is the corresponding sampled noise vector. Equation (5) can be equivalently written as

$$\begin{aligned}\mathbf{y}_r &= \bar{\mathbf{F}}_r\bar{\mathbf{x}}_r + \mathbf{n} \\ &= \begin{bmatrix}\mathbf{f}_r(\bar{\mathbf{r}}_0) & \mathbf{f}_r(\bar{\mathbf{r}}_1) & \cdots & \mathbf{f}_r(\bar{\mathbf{r}}_{K-1})\end{bmatrix}\bar{\mathbf{x}}_r + \mathbf{n}\end{aligned} \quad (8)$$

where $$\bar{\mathbf{x}}_r \triangleq \begin{bmatrix}\bar{x}_0 & \bar{x}_1 & \cdots & \bar{x}_{K-1}\end{bmatrix}^T , \quad (9)$$

and $\bar{\mathbf{F}}_r$ is $NM_R \times K$, with each column given by

$$\begin{aligned}\mathbf{f}_r(\bar{\mathbf{r}}_k) &= \left[\mathbf{P}\mathbf{a}(\bar{\mathbf{r}}_k)\right] \otimes \mathbf{b}(\bar{\mathbf{r}}_k) & (10)\\ &= \left[\mathbf{P}\otimes\mathbf{I}_{M_R}\right]\left[\mathbf{a}(\bar{\mathbf{r}}_k)\otimes\mathbf{b}(\bar{\mathbf{r}}_k)\right] \, . & (11)\end{aligned}$$

A typical radar application forms an image from the measured data; this means recovering not only the reflectances $\bar{x}_k$, but also the directions $\bar{\mathbf{r}}_k$. Frequently, those directions are obtained by beamforming techniques or by spectral DOA estimation methods, just like the MUSIC or the ESPRIT [6]. On the other hand, beamforming can be understood as probing each direction $\mathbf{r}_g$ at a fine grid defined by $G \geq K$ directions containing all targets, meaning that $\{\mathbf{r}_g | 0 \leq g \leq G\} \supseteq \{\bar{\mathbf{r}}_k | 0 \leq k \leq K\}$. In this sense, (8) can be replaced by:

$$\begin{aligned}\mathbf{y}_r &= \mathbf{F}_r\mathbf{x}_r + \mathbf{n} & (12)\\ &= \begin{bmatrix}\mathbf{f}_r(\mathbf{r}_0) & \mathbf{f}_r(\mathbf{r}_1) & \cdots & \mathbf{f}_r(\mathbf{r}_{G-1})\end{bmatrix}\mathbf{x}_r + \mathbf{n} & (13)\end{aligned}$$

where $\mathbf{x}_r \triangleq \begin{bmatrix}x_0 & x_1 & \cdots & x_{G-1}\end{bmatrix}^T$ is a sparse vector with K non-zero entries, corresponding to the values of $\bar{\mathbf{x}}_r$ for which the directions $\bar{\mathbf{r}}_k$ and $\mathbf{r}_g$ coincide. Hence, finding the target directions is equivalent to recovering the support of $\mathbf{x}_r$.

Remark: In general, the assumption that all targets lie in a fine grid is not satisfied in practice, implying in a "gridding error" from the design point of view. Still, it is argued in [8] that while recovery depends on the noise level, in a noiseless setup the overall error bears a linear relation with the total perturbation introduced in $\mathbf{F}_r$ by the use of an incorrect grid.

3. JOINT RANGE/CROSS-RANGE MODEL

The model presented in the previous section considers all targets as belonging to a single range. For multiple ranges, $\mathbf{x}_r$ becomes a function of the range delay τ_r, so that the received signal must be written as a convolution integral:

$$\mathbf{y}_r(t) = \int \sum_{k=0}^{K-1} x_k(\tau_r)\mathbf{b}(\bar{\mathbf{r}}_k)\left[\mathbf{p}^T(t-2\tau_r)\mathbf{a}(\bar{\mathbf{r}}_k)\right]\mathrm{d}\tau_r \ + \ \mathbf{n}(t) \quad (14)$$

Sampling $\mathbf{y}_r(t)$ at t_s, and defining $\tau_n \triangleq \tau_0 - nt_s/2$, assuming that all targets are confined to Q range bins, we can write (14) as $\mathbf{y} = \mathcal{F}\mathbf{x}$, where $\mathcal{F}$ is $M_R(N+Q-1)\times QG$ block-Toeplitz matrix, which for convenience we partition into block columns:

$$\mathcal{F} = \begin{bmatrix}\mathcal{F}_0 & \mathcal{F}_1 & \cdots & \mathcal{F}_{Q-1}\end{bmatrix} . \quad (15)$$

Each $\mathcal{F}_n$ now has the same structure of $\mathbf{F}_r$, and its columns can be obtained by replacing $\mathbf{P}$ in Eq. (11) by their zero-padded versions, say, $\mathcal{P}_n \triangleq \begin{bmatrix}\mathbf{0}_{M_T\times n} & \mathbf{P}^T & \mathbf{0}_{M_T\times(Q-1)-n}\end{bmatrix}^T$.

Recovering the support of the vector $\mathbf{x}$ in this model thus determines not only the directions of arrival, but also the range bins containing the desired targets.

4. COMPRESSED SENSING IMAGING

Obtaining $\mathbf{x}$ from $\mathbf{y}$ is complicated due to the low rank nature of $\mathcal{F}$. Because each of its columns have at most $M_T M_R$ degrees of freedom, $rank(\mathcal{F}_r) \leq M_T M_R$, an ill-conditioned situation even for long pulses. However, since $\mathbf{x}$ is sparse, compressed sensing [9] can be readily used to estimate it.

The accurate recovery of $\mathbf{x}$ depends on the mutual coherence of the columns of $\mathcal{F}$, defined by

$$\mu(\mathcal{F}) \triangleq \max_{\ell\neq h} \frac{\left|[\mathcal{F}]_\ell^* \, [\mathcal{F}]_h\right|}{\|[\mathcal{F}]_\ell\|_2\|[\mathcal{F}]_h\|_2} \, , \quad (16)$$

with * denoting complex conjugate transposition, and where $\|[\mathcal{F}]_\ell\|_2$ denotes the Euclidean norm of the ℓ-th column of $\mathcal{F}$.

It can be shown that, given $\mu(\mathcal{F})$, we can recuperate

$$K < \frac{1}{2}\left(1 + \frac{1}{\mu(\mathcal{F})}\right) \tag{17}$$

elements of $\mathbf{x}$ perfectly [9].

To compute the mutual coherence one can take advantage of the structure of $\mathcal{F}$, whose Gram matrix becomes block-Toeplitz. In this case, each such block is given by

$$\begin{aligned}[\mathcal{F}_l^* \mathcal{F}_m]_{i,j} &= \{[\mathcal{P}_l \otimes \mathbf{I}_{M_R}]\,\mathbf{c}_i\}^* \{[\mathcal{P}_m \otimes \mathbf{I}_{M_R}]\,\mathbf{c}_j\} && (18)\\ &= \mathbf{c}_i^* \left[\mathbf{R}(l-m) \otimes \mathbf{I}_{M_R}\right]\mathbf{c}_j && (19)\end{aligned}$$

where $\mathbf{R}(l-m) \triangleq \mathcal{P}_l^* \mathcal{P}_m$ is the pulse vector autocorrelation function, and $\mathbf{c}_i \triangleq \mathbf{a}(\mathbf{r}_i) \otimes \mathbf{b}(\mathbf{r}_i)$ for compactness of notation. Let $k = l - m$, so that $\mathbf{G}(k) \triangleq \mathbf{R}(k) \otimes \mathbf{I}_{M_R}$. Then, the coherence measure (16) can be equivalently written as

$$\mu(\mathcal{F}) = \max_{i \neq j \vee k \neq 0} \frac{\mathbf{c}_i^* \mathbf{G}(k) \mathbf{c}_j}{\left[\mathbf{c}_i^* \mathbf{G}(0) \mathbf{c}_i\right]^{1/2} \left[\mathbf{c}_j^* \mathbf{G}(0) \mathbf{c}_j\right]^{1/2}} . \tag{20}$$

Observe that in minimizing the above quotient, we have freedom to select both the MIMO correlation function and the manifold directions. Because exact (weighted) orthogonality of the manifold vectors can only be attained at one particular lag k, we can adopt the following procedure.

For the lag $k = 0$, we pick a set of directions such that $\mathbf{c}_i$ and $\mathbf{c}_j$ annihilates (20) for a given $i \neq j$; For $k \neq 0$, we would like to design $\mathbf{G}(k)$ as close to the null matrix as possible. That is, for $k = 0$ the numerator in (20) is given by

$$[\mathcal{F}_l^* \mathcal{F}_l]_{i,j} \;=\; [\mathbf{a}^*(\mathbf{r}_i)\mathbf{R}(0)\mathbf{a}(\mathbf{r}_j)]\,[\mathbf{b}^*(\mathbf{r}_i)\mathbf{b}(\mathbf{r}_j)] \tag{21}$$

which represents the product between the receiver beampattern, i.e., $\Upsilon_{RX}(\mathbf{r}_i, \mathbf{r}_j) \triangleq \mathbf{b}^*(\mathbf{r}_i)\mathbf{b}(\mathbf{r}_j)$, and the weighted beampattern of the transmitter, defined as $\Upsilon_{TX}(\mathbf{r}_i, \mathbf{r}_j) \triangleq \mathbf{a}^*(\mathbf{r}_i)\mathbf{R}(0)\mathbf{a}(\mathbf{r}_j)$. The fact is that for some array geometries, it is possible to choose directions where either beampatterns are zero; the number of selected directions defines the dimension G of the grid. The simplest choice is to enforce $\mathbf{R}(0) = N\mathbf{I}$, which ensures that all the pulses have the same power and are orthogonal at the zero lag. As a result, this choice also simplifies the design of the transmitting array.

One array geometry that offers a simple selection of directions is the uniform linear array (ULA) [6], composed by M equally spaced elements, which can be aligned with the z-axis. The direction vectors can be entirely represented by the arrival angles $\{\phi_i, \phi_j\} \in [-\pi/2, \pi/2]$, so that the receiving beampattern vector can be written more explicitly as

$$\Upsilon_{RX}(\phi_i, \phi_j) = e^{-j\frac{2\pi}{\lambda_0}\psi_{ij} q_z} \frac{\sin\left(\frac{2\pi}{\lambda_0}\psi_{ij}\frac{M_R d_R}{2}\right)}{\sin\left(\frac{2\pi}{\lambda_0}\psi_{ij}\frac{d_R}{2}\right)} \tag{22}$$

where $\psi_{ij} \triangleq \sin(\phi_i) - \sin(\phi_j)$, q_z is the z-axis coordinate of the center of the array, and d_R is the distance between the array elements. Usually, one chooses d_R as $\lambda_0/2$; this choice induces a single main lobe and $M_R - 1$ zeros in the beampattern. Similar reasoning can be carried out for the transmitting array beampattern, just by changing the corresponding parameters accordingly.

Moreover, it is possible to select different spacings for both arrays. For instance, by setting the distance between the elements of the transmitting array to $d_T = d_R M_R$, the combined trasmit/receive elements collapse to the virtual ULA arrangement described in [2]. If $d_R = \lambda_0/2$, the combined patterns will generate $M_T M_R - 1$ possible angles ϕ_j for each selected angle ϕ_i. For such arrangement, we can pick a grid of $G = M_T M_R$ angles, namely, $\phi_g = \phi_0 + g\delta_g$, where $\delta_g \triangleq \arcsin(2g/M_R M_T)$, and $g \in \mathbb{Z}$, $g \in [0, G)$. Note that exchanging the receive and transmit arrays does not alter the resulting choice of angles.

Now, introduce the Cholesky factorization $\mathbf{G}(0) = \mathbf{L}\mathbf{L}^*$, and define $\bar{\mathbf{c}}_i \triangleq \mathbf{L}^* \mathbf{c}_i$. For a correlation lag $k \neq 0$, the ratio in (20) can be written as

$$\max_{i \neq j \vee k \neq 0} \frac{\bar{\mathbf{c}}_i^* \mathbf{L}^{-1} \mathbf{G}(k) \mathbf{L}^{-*} \bar{\mathbf{c}}_j}{\|\bar{\mathbf{c}}_i\|_2 \|\bar{\mathbf{c}}_j\|_2} \tag{23}$$

which assumes the form of the well known *Rayleigh quotient* (see, e.g., 9.8.36 in [10]), however, one for every $\mathbf{G}(k)$. A simple upper bound for (23) is

$$\lambda_{\max}(\mathbf{L}^{-1}\mathbf{G}(k)\mathbf{L}^{-*}) \tag{24}$$

in terms of the maximum eigenvalue $\lambda_{\max}(\cdot)$. Since we have that $\lambda_{\max}(\mathbf{L}^{-1}\mathbf{G}(k)\mathbf{L}^{-*}) \leq \|\mathbf{L}^{-1}\mathbf{G}(k)\mathbf{L}^{-*}\|_F = \|\mathbf{G}^{-1}(0)\mathbf{G}(k)\|_F = M_R^{1/2}\|\mathbf{R}^{-1}(0)\mathbf{R}(k)\|$, and $\mathbf{R}(0)$ is finite, this requires ideally, $\mathbf{R}(k)$ as a null matrix for all $k \in [1, Q)$.

Independent Gaussian sequences sets, as considered in [5], allows us to approximate the above requirements, i.e., $\mathbf{R}(0) = N\mathbf{I}$ and $\mathbf{R}(k) = 0$, in a stochastic sense, but these may demand a high level of synchronization (as well as an increase in mutual coherence as we shall see next). As an alternative, in this paper we make use of the so-called *complementary sequences sets*, which can be generated by optimizing the following block LS criterion (see Eq. (11) in [3]):

$$\min_{\mathbf{R}(k)} \;\|\mathbf{R}(0) - N\mathbf{I}_{M_T}\|_F^2 + 2\sum_{k=1}^{Q-1} \|\mathbf{R}(k)\|_F^2 \tag{25}$$

One advantage of working with complementary sequences is that we can produce zero correlations in a range of only $Q - 1$ samples, yielding lower cross-correlation within the same range when compared to its Gaussian sequences counterpart. Note that it is also possible to restrict the pulse samples to specific modulations, such as QAM or BPSK.

5. NUMERICAL EXAMPLE

We consider a MIMO radar system which comprises $M_T = 5$ transmitting and $M_R = 11$ receiving antennas, in a virtual

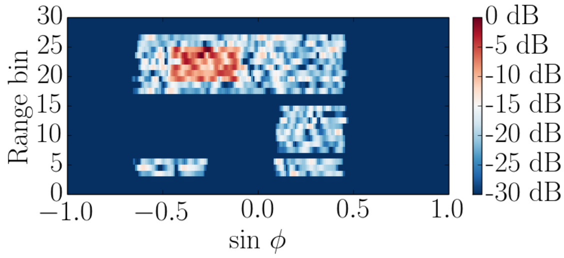

(a) LASSO Compressed Sensing

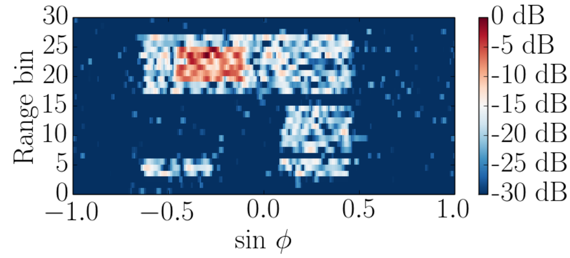

(c) LASSO Compressed Sensing

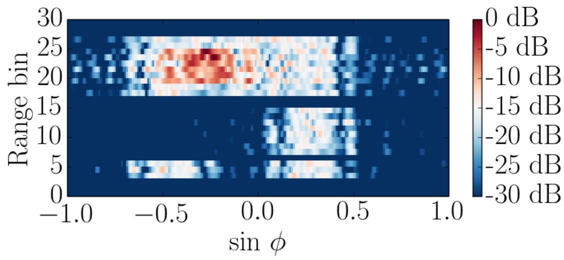

(b) Least Squares

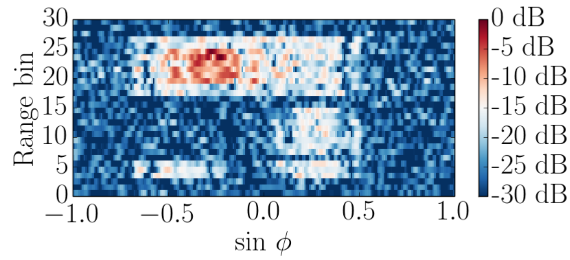

(d) Least Squares

Fig. 3. Reconstructed images with (a) and (b) SNR = 20 dB, (c) and (d) SNR = 5 dB, using complementary sequences.

ULA configuration. For this scenario, we have employed the WeCAN algorithm [3] to design a complementary set of sequences which minimizes (25) with a length $N = 256$, and for $Q = 48$ low cross-correlation samples.

The exact target image for the experiments is shown in Fig. 2. We restricted the targets to be within 30 range bins, while the visible area $\phi \in [-\pi/2, \pi/2)$ was divided into 220 cross-range directions, such that $\sin\phi$ is equally spaced.

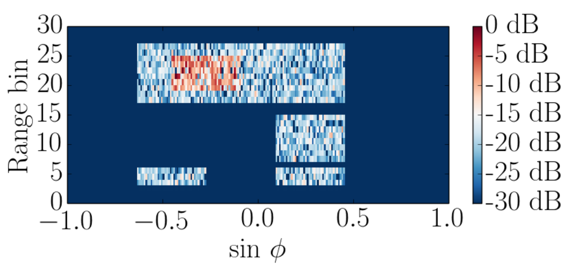

Fig. 2. True target image.

This virtual ULA allows us to construct a grid composed of $G = 55$ directions, which is less dense than the true targets grid. We circumvented this issue by dividing the target grid into four interleaved direction grids of the same number $G = 55$. For this setup, we obtained $\mu(\mathcal{F}) \approx 0.014$. The recovery algorithm used was the ℓ_1-regularized least-squares, well known as the LASSO algorithm [11] in order to retrieve the target support. Figure 3(a) shows the resulting image for a signal-to-noise ratio, i.e., SNR = 20 dB; in contrast, Fig. 3(b) shows the result when a LS beamformer is applied at individual ranges, as in [3]. Figures 3(c) and 3(d) show the analogous images when SNR = 5 dB. In order to compare our results with the ones that would be produced by independent Gaussian sequences as in [5], we illustrate the resulting image for the latter in Fig. 4. In this case, the mutual coherence is increased by one order of magnitude, i.e., $\mu(\mathcal{F}) \approx 0.15$, which visually degrades robustness when compared to Fig. 3(c).

We remark that despite the fact our model was developed considering point targets, these numerical examples show that we have good image recovering even in the case of extended targets. By scanning through interleaved grids, we were able to further improve the target edge detection.

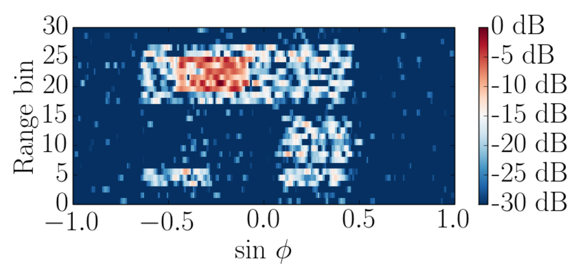

Fig. 4. Image formed via LASSO, using Gaussian sequences (SNR = 5 dB).

6. CONCLUDING REMARKS

In this paper we have proposed a design procedure for a full 3D compressed sensing matrix in a MIMO radar scenario. Even in a noisy environment, the image reconstruction was adequate, outperforming traditional LS beamformation. The MIMO pulse cross-correlation along with the complementary sequences design borrowed from [3] were crucial when minimizing the mutual coherence of the system, and performed favorably in comparison to the Gaussian pulses based design.

7. REFERENCES

[1] E. Fishler, A. Haimovich, R. Blum, D. Chizhik, L. Cimini, and R. Valenzuela, "MIMO radar: an idea whose time has come," in *Radar Conference, 2004. Proceedings of the IEEE*, 2004, pp. 71–78.

[2] J. Li, P. Stoica, L. Xu, and W. Roberts, "On parameter identifiability of MIMO radar," *Signal Processing Letters, IEEE*, vol. 14, no. 12, pp. 968–971, 2007.

[3] H. He, P. Stoica, and J. Li, "Designing unimodular sequence sets with good correlations - including an application to MIMO radar," *Signal Processing, IEEE Transactions on*, vol. 57, no. 11, pp. 4391–4405, Nov 2009.

[4] M. Rossi, A. M. Haimovich, and Y. C. Eldar, "Spatial compressive sensing for MIMO radar," *CoRR*, vol. abs/1304.4578, 2013, submitted to IEEE Transactions on Signal Processing, Apr. 2013.

[5] T. Strohmer and B. Friedlander, "Analysis of sparse MIMO radar," *CoRR*, vol. abs/1203.2690, 2012.

[6] H. L. Van Trees, *Optimum Array Processing (Detection, Estimation, and Modulation Theory, Part IV)*, Wiley-Interscience, 1 edition, Mar. 2002.

[7] M. Cheney, "A mathematical tutorial on synthetic aperture radar," *SIAM Rev.*, vol. 43, no. 2, pp. 301–312, Feb. 2001.

[8] M. A. Herman and T. Strohmer, "General deviants: An analysis of perturbations in compressed sensing," *Selected Topics in Signal Processing, IEEE Journal of*, vol. 4, no. 2, pp. 342–349, April 2010.

[9] Y. C. Eldar and G. Kutyniok, Eds., *Compressed Sensing: Theory and Applications*, Cambridfe University Press, 2012.

[10] D. S. Bernstein, *Matrix Mathematics: Theory, Facts, and Formulas*, Princeton University Press, 2nd edition, 2009.

[11] R. Tibshirani, "Regression shrinkage and selection via the Lasso," *Journal of the Royal Statistical Society, Series B*, vol. 58, pp. 267–288, 1994.